ELSEVIER

Journal of Molecular Catalysis A: Chemical 197 (2003) 193–205

JOURNAL OF MOLECULAR CATALYSIS A: CHEMICAL

www.elsevier.com/locate/molcata

Effects of CuO/CeO_2 and $CuO/\gamma\text{-}Al_2O_3$ catalysts on NO + CO reaction

Jiang Xiaoyuan [a,*], Lou Liping [b], Chen Yingxu [b], Zheng Xiaoming [a]

[a] *Institute of Catalysis, The Faculty of Science, Zhejiang University, Hangzhou 310029, PR China*

[b] *Institute of Environmental Engineering, The Faculty of Environment and Resource, Zhejiang University, Hangzhou 310029, PR China*

Received 19 May 2002; accepted 18 October 2002

Abstract

Reducibility and characteristics of CeO_2, $\gamma\text{-}Al_2O_3$, CuO/CeO_2, $CuO/\gamma\text{-}Al_2O_3$ and ceria-modified $CuO/\gamma\text{-}Al_2O_3$ catalysts were examined using a microreactor-GC NO + CO reaction system and the methods of BET, XRD, TPR, XPS and NO-TPD. The results showed that the catalytic activities of CuO/CeO_2 and $CuO/\gamma\text{-}Al_2O_3$ were increased compared to that of CeO_2 or $\gamma\text{-}Al_2O_3$ alone, probably due to the presence of the copper oxide species with low valence and surface dispersion. There were two TPR peaks of CuO/CeO_2, a low-temperature peak due to the reduction of highly dispersed copper oxide species and a high-temperature peak due to the reduction of bulk CuO. $CuO/\gamma\text{-}Al_2O_3$ had one TPR peak, while the CeO_2-modified $CuO/\gamma\text{-}Al_2O_3$ had three reduction peaks with one low-temperature peak and two high-temperature peaks. The Cu $2p_{3/2}$ (eV) binding energy of 5.0 wt.% CuO/CeO_2 was 932.79 to 934.11 eV, compared to that of $CuO/\gamma\text{-}Al_2O_3$ equal to 935.0 eV. After added with CeO_2, the Cu $2p_{3/2}$ (eV) binding energy was 934.1 eV, slightly lower than the Cu $2p_{3/2}$ (eV) binding energy. During the thermal desorption of NO, five desorption species (NO, N_2O, N_2, O_2 and NO_2) were adsorbed on CeO_2 and $\gamma\text{-}Al_2O_3$ but only four desorption species (NO, N_2O, N_2 and NO_2) adsorbed on CuO/CeO_2 and $CuO/\gamma\text{-}Al_2O_3$. Two adsorbing states of NO were observed on the catalyst's surface, the weak one at low temperatures and the strong one at high temperatures. The NO-TPD profile also showed that peak temperatures of NO desorption by the catalysts were lower than that by the supports, indicating that the NO decomposition activity of the catalysts was higher than that of the supports.

Keywords: CeO_2; $\gamma\text{-}Al_2O_3$; CuO/CeO_2; $CuO/\gamma\text{-}Al_2O_3$; NO + CO reaction

1. Introduction

Nitric oxide (NO) and carbon monoxide (CO) are largely produced by the combustion of fossil fuels from vehicles and stationary sources, which results in serious environmental problems such as acid rains and photochemical smog. The NO + CO reaction is very important in catalytic control of vehicle emissions [1]. Early studies on NO reduction using copper-containing catalysts have been reported [2,3]. Cupric oxide (CuO) and alumina-supported copper oxides ($CuO/\gamma\text{-}Al_2O_3$) have been tested for their catalytic activities of NO reduction in the presence of CO [4]. In recent years, most of the studies have focused on precious metal catalysts for the reduction of NO in the presence of CO [5,6]. The NO + CO reaction by alumina-supported rhodium catalysts doped with ceria or ceria-supported rhodium catalysts has also received high attention [7]. Further, the catalytic activities of alumina- or ceria-supported platinum along with Pt–Rh bimetallic particles have been examined

* Corresponding author.
E-mail address: xyjiang@mail.hz.zj.cn (J. Xiaoyuan).

1381-1169/02/$ – see front matter © 2002 Elsevier Science B.V. All rights reserved.
PII: S1381-1169(02)00587-3

[8]. Muraki et al. [9] examined the effect of La_2O_3 on NO reduction by alumina-supported palladium catalysts and found that addition of La_2O_3 increased the reduction activity. However, the employment of precious metal catalysts is limited due to their scarcity and high cost. The catalysts containing transition metals and rare earth elements such as V, Cu, Cr, Co, Ce and La with unique catalytic properties have been considered as a substitute for the precious metals and have recently attracted much interest [10].

Copper-supported catalyst is one of the most promising catalysts in reactions with nitrogen oxides, especially in selective catalytic reduction of NO with ammonia [11] and reduction with CO [12]. The Cu/ZSM-5 catalyst is also a classical one with respect to NO decomposition and selective catalytic reduction of NO with hydrocarbons, although at present it is far from practical application. In this paper, the activities of CuO/CeO_2, $CuO/\gamma\text{-}Al_2O_3$ and $CuO\text{-}CeO_2/\gamma\text{-}Al_2O_3$ were measured using a microreactor-GC NO + CO reaction system, and their properties were characterised with the BET, XRD, TPR, XPS and NO-TPD procedures.

2. Experimental

2.1. Catalyst preparation

The supports were CeO_2 and $\gamma\text{-}Al_2O_3$. CeO_2 was prepared by thermal decomposition of $Ce(NO_3)_3$ at 650 °C for 4 h. $\gamma\text{-}Al_2O_3$ was provided by Wenzhou Alumina Factory in China and was calcined at 500 °C for 4 h in air before being used as a support. The CuO/CeO_2, $CuO/\gamma\text{-}Al_2O_3$ and $CuO\text{-}CeO_2/\gamma\text{-}Al_2O_3$ catalysts were prepared by the impregnation method using $Cu(NO_3)_2$ and $Ce(NO_3)_3$ aqueous solutions of the desired concentrations. These catalysts were dried at 120 °C for 12 h, followed by calcination in an air stream at 500 °C for 2 h.

2.2. The activity of catalysts

Catalytic activity was determined under the steady state in a fixed-bed quartz reactor ($\phi = 6$ mm). The particle size of catalysts was 20–40 mesh, and 120 mg of the catalysts were used. The reaction gas (i.e. feed steam) consisted of a fixed composition of 6.0% NO, 6.0% CO and 88% He (v/v) as a dilute. The catalysts were pretreated using the reaction gas at 500 °C for 1 h. After being cooled to room temperature, the catalysts were allowed to react with the mixed gas. The reactions were operated at different temperatures with a space velocity of 5000 h^{-1}. Two volumes and thermal conduction detectors were used for analysing the catalytic activity. Volume A was packed with 13X molecular sieve for separating N_2, NO and CO, and Volume B was packed with Paropak Q for separating N_2O and CO_2. The catalytic activity was calculated using the following formula:

$$[\mathrm{NO}]_{\mathrm{conv.}} = \frac{[\mathrm{NO}]_{\mathrm{in}} - [\mathrm{NO}]_{\mathrm{out}}}{[\mathrm{NO}]_{\mathrm{in}}}$$

$$[\mathrm{N_2}]_{\mathrm{sel.}} = \frac{2[\mathrm{N_2}]}{[\mathrm{NO}]_{\mathrm{in}} - [\mathrm{NO}]_{\mathrm{out}}}$$

2.3. Measurements

The BET surface area of catalysts was determined by N_2 adsorption at 77 K using a Coulter OMNISORP-100 instrument.

H_2-temperature programmed reduction (TPR) was done by gas chromatography (GC) method using a thermal conductivity detector. The sample (5–10 mg) was activated in an O_2 stream at 500 °C for 0.5 h. After it was cooled to 30 °C, H_2-TPR was conducted. The reduction gas was a mixture of H_2 and N_2 at 99.999% purity and had an H_2 concentration of 5%. Both H_2 and N_2 were purified using a 401 deoxidiser and silica gel. The flow rate of the H_2/N_2 mixture was 18 ml min^{-1} ($\beta = 20$ K min^{-1}).

X-ray diffraction (XRD) data were obtained at 25 °C using a horizontal Rigaku B/Max IIIB powder diffractometer with Cu Kα radiation and a power of 40 × 30 mA. The diffraction angles were 2θ (°). The wavelength of the source used was Cu Kα = 1.540598 Å.

X-ray photoelectron spectroscopy (XPS) spectra were recorded on an America PHI-550 Spectrometer with Al Kα radiation (1486.6 eV). The calibration of the spectrometer energy scale was performed using gold (Au $4f_{7/2}$ = 83.8 eV). The C 1s line at 284.6 eV was used as an internal standard for correction of binding energies. The accuracy of energy values was ±0.3 eV.

For the measurement of NO-temperature programmed desorption (TPD), 250 mg of fresh catalysts were loaded onto a quartz reactor ($\phi = 5$ mm), and reduced in the reaction gas (6% NO, 6% CO and 88% He) at 500 °C for 1.0 h, followed by heating in He at 600 °C for 1.0 h. After being cooled to 40 °C in a flow of He, the catalysts were exposed to a 10% NO–He mixture gas. Excessive NO was removed, and the catalysts were remained in the He flow until no significant amount of adsorbates could be detected. The catalysts were then ramped to 800 °C at a linear heating rate of 20 °C min^{-1} in the He flow. The effluent gases were analysed with a mass spectrometer.

3. Results and discussion

3.1. BET surface area of catalysts

As shown in Table 1, the BET surface areas were 54.712 m^2 g^{-1} for the obtained CeO_2 and 274.301 m^2 g^{-1} for γ-Al_2O_3. When the amount of CuO loading increased from 1.0 to 15.0 wt.%, the BET surface area of the CuO/CeO_2 catalyst decreased from 49.902 to 44.798 m^2 g^{-1}. The BET surface areas of the CuO/γ-Al_2O_3, CuO-CeO_2/γ-Al_2O_3 catalysts also decreased with the increase in CuO loading. In addition, the BET surface areas of the CuO/CeO_2 and CuO/γ-Al_2O_3 were all smaller than that of supports CeO_2 and γ-Al_2O_3 (Table 1).

Table 1
BET surface area of different catalysts

Catalysts	Calcination		BET surface area (m^2 g^{-1})
	Temperature (°C)	Time (h)	
CeO_2	650	4	54.712
γ-Al_2O_3	500	4	274.301
1.0% CuO/CeO_2	500	2	49.902
5.0% CuO/CeO_2	500	2	48.240
10.0% CuO/CeO_2	500	2	44.543
15.0% CuO/CeO_2	500	2	44.798
10.0% CuO/CeO_2	800	2	25.324
10.0% CuO/CeO_2	900	2	11.217
1.0% CuO/γ-Al_2O_3	500	2	264.345
5.0% CuO/γ-Al_2O_3	500	2	258.963
10.0% CuO/γ-Al_2O_3	500	2	249.724
10.0% CuO/γ-Al_2O_3	800	2	177.511
10.0% CuO-2.0% CeO_2/γ-Al_2O_3	500	2	231.924
10.0% CuO-10.0% CeO_2/γ-Al_2O_3	500	2	203.198

3.2. The activities of catalysts for NO + CO reaction

The effects of CuO loading on NO conversions are shown in Fig. 1. At 250 °C, NO conversions by CuO/CeO_2 catalysts reached 82 and 99.8% when the amount of CuO loading was 1.0 and 5.0 wt.%, respectively. However, NO conversions decreased steadily with further increase in CuO loading. Excessive

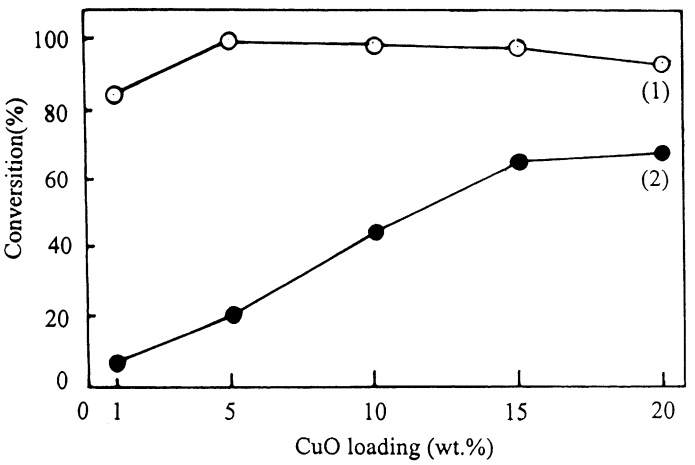

Fig. 1. Response of NO conversions to CuO loading amount. (1) CuO/CeO_2; (2) CuO/γ-Al_2O_3.

copper resulted in formation of crystalline phase of CuO, causing a decrease in active phase species number and consequently reduced the catalytic activity. NO conversions by $CuO/\gamma\text{-}Al_2O_3$ catalysts at 250 °C also increased with the increase in CuO loading, but the conversions only reached 71% when the CuO loading amount was 20.0 wt.%. These results indicate that the activity of CuO/CeO_2 are much better than that of $CuO/\gamma\text{-}Al_2O_3$ and prove that the effects of CuO loading on the catalytic activities are related to the characters and specific surface areas of the supports [16]. More importantly, it was found that addition of CeO_2 to $CuO/\gamma\text{-}Al_2O_3$ induced a prompt increase in catalytic activity of NO + CO reaction. This was probably due to the interaction between CeO_2 and $\gamma\text{-}Al_2O_3$, which resulted in a formation of $CeAlO_3$, Cu^+ and Cu^0 and consequently a high activity of $CuO\text{-}CeO_2/\gamma\text{-}Al_2O_3$.

After the $CuO/\gamma\text{-}Al_2O_3$ catalysts were calcined at 800 °C for 2 h, their activities changed badly (Fig. 2). The XRD analysis showed a solid phase reaction between CuO and $\gamma\text{-}Al_2O_3$, which produced a surface spinel structure of $CuAl_2O_4$. The formation of $CuAl_2O_4$ was unfavourable for NO + CO reaction. However, addition of CeO_2 to $CuO/\gamma\text{-}Al_2O_3$ was able to restrain the interaction between CuO and $\gamma\text{-}Al_2O_3$ and the $CuAl_2O_4$ formation. As a result, the effects of high-temperature sintering were reduced and the catalytic activity was maintained.

Table 2 shows the effects of reaction temperature on NO, CO conversions and N_2 selectivities for NO+CO reaction by CuO/CeO_2 and $CuO/\gamma\text{-}Al_2O_3$ catalysts. The NO and CO concentrations decreased simultaneously, but N_2 and CO_2 increased as the reaction temperatures increased. At 50 °C, little amount of N_2, CO_2 and N_2O was detected in the reaction products. At 100 °C, the amount of N_2, CO_2 and N_2O increased and the conversions of NO and CO increased promptly. A continuous increase in N_2 and CO_2 but a decrease in N_2O was observed at 200 °C, together with the conversions of NO and CO being 94.8 and 73.9%, respectively. At 250 °C, the NO + CO reactions tended to complete and the N_2 selectivities by CuO/CeO_2 and $CuO/\gamma\text{-}Al_2O_3$ catalysts were 100 and 46.7%, respectively. The results indicate that N_2O was formed during the initial stage at lower temperatures, and with the increase in temperature the amount of N_2O reached a maximum. Further increase in temperature, however, caused a gradual decrease in the amount of N_2O until reaching zero. In contrast, the amount of N_2 increased continuously with the increase in temperature.

3.3. XRD analysis of crystal phase of catalysts

XRD patterns of CuO/CeO_2 catalysts with different CuO loading amounts were shown in Fig. 3. A diffraction peak of CeO_2 at 2θ 28.5, 33.1–47.5° was observed when CuO loading was less than 5.0 wt.%,

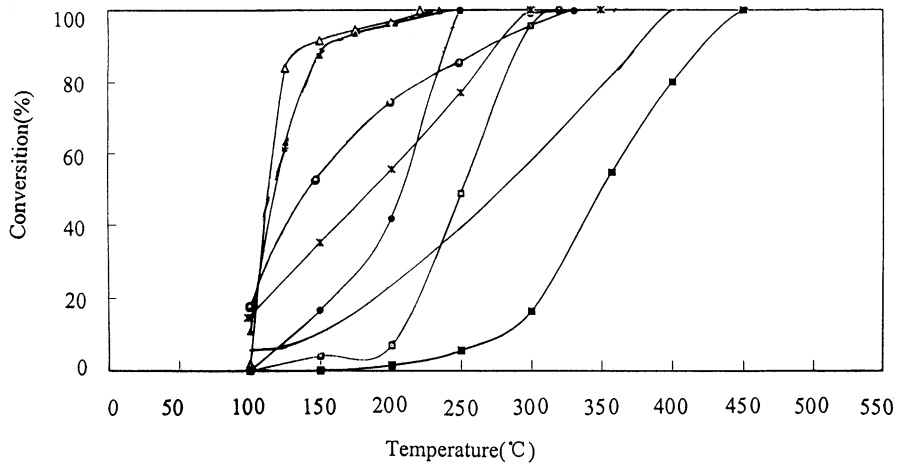

Fig. 2. NO + CO reaction activity of the catalysts. (●) 10% CuO/CeO_2; (△) 5.0% CuO/CeO_2; (▲) 10.0% CuO/CeO_2; (—) 10.0% $CuO/\gamma\text{-}Al_2O_3$; (■) 10.0% $CuO/\gamma\text{-}Al_2O_3$ (800 °C, 2 h); (□) 10.0% CuO-10.0% $CeO_2/\gamma\text{-}Al_2O_3$ (800 °C, 2 h); (○) 10.0% CuO-10.0% $CeO_2/\gamma\text{-}Al_2O_3$; (×) 10.0% CuO-2.0% $CeO_2/\gamma\text{-}Al_2O_3$.

Table 2
Effects of temperature on NO, CO conversions and N_2 selectivities for NO + CO reaction by CuO/CeO_2 and $CuO/\gamma\text{-}Al_2O_3$ catalysts

Temperature (°C)	Conversion (%)				N_2 selectivities (%)	
	CuO/CeO_2		$CuO/\gamma\text{-}Al_2O_3$		CuO/CeO_2	$CuO/\gamma\text{-}Al_2O_3$
	NO	CO	NO	CO		
50	4.7	5.7	2.1	1.2	2.7	1.9
100	67.8	44.2	4.9	3.7	10.7	21.5
150	86.6	43.5	3.1	5.1	12.7	33.6
200	94.8	73.9	21.9	20.4	77.9	35.7
250	99.8	96.7	38.2	21.8	100	46.7
300	100	98.4	34.8	17.6	100	100
350	100	98.9	68.0	50.1	100	100
400	100	97.5	100	89.7	100	100
500	100	97.1	100	97.1	100	100
600	100	97.7	100	94.6	100	100

compared to two diffraction peaks of CuO between 2θ 35.5 and 38.7° in addition to the diffraction peak of CeO_2 at CuO loading of greater than 5.0 wt.%. The diffraction peak increased with the increase in CuO loading, indicating a change of CuO dispersion. After calcination at 800 and 900 °C for 2 h, the diffraction peaks of CuO and CeO_2 were even sharper, i.e. the crystalline of CuO and CeO_2 became more integrity.

The TPR profiles of pure CeO_2 and different components of CuO loaded with CeO_2 are shown in Fig. 4. Two reduction peaks of pure CeO_2 were found at 430 and 570 °C. We presume that the low-temperature peak was due to the reduction of CeO_2 surface oxygen, and the high-temperature peak was due to the reduction of bulk oxygen. In addition, the TPR profiles show two reduction peaks for all the CuO/CeO_2 catalysts—the existence of two CuO species. One species represented small and highly dispersed CuO particles interacting with CeO_2 at low temperature, and the other species represented larger particle bulk CuO interacting with CeO_2 at high temperature. The low-temperature peak was at 210 °C at the CuO loading of 1.0 wt.%. Increasing CuO loading caused the reduction peak shifting towards the

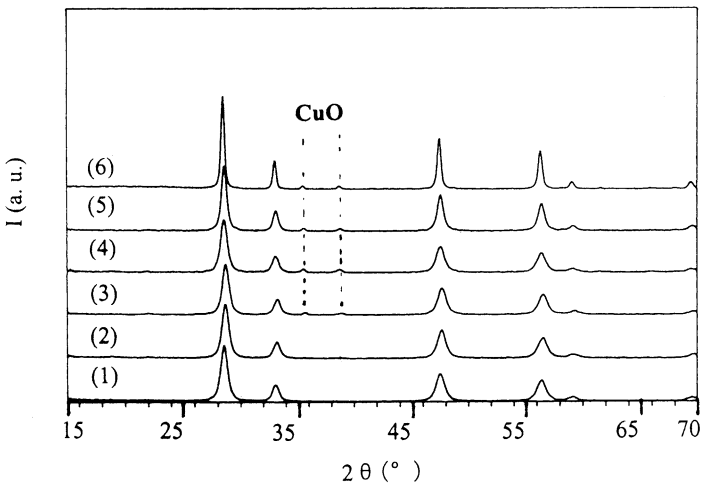

Fig. 3. XRD patterns of CuO/CeO_2 catalyst. (1) 1.0% CuO/CeO_2; (2) 5.0% CuO/CeO_2; (3) 10.0% CuO/CeO_2; (4) 15.0% CuO/CeO_2; (5) 10.0% CuO/CeO_2 (800 °C, 2 h); (6) 10.0% CuO/CeO_2 (900 °C, 2 h).

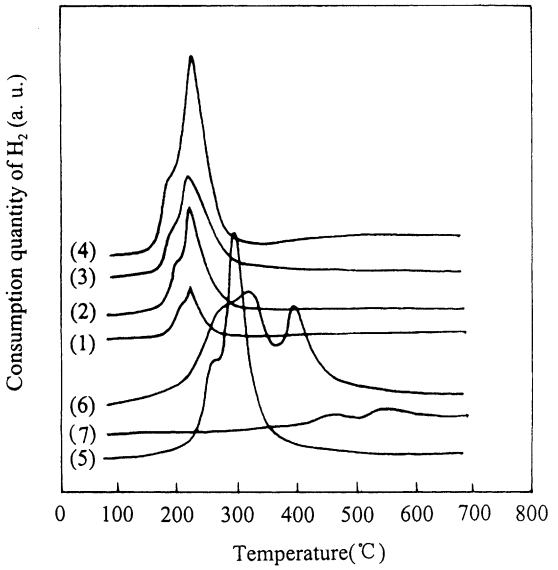

Fig. 4. TPR patterns of CuO/CeO_2 catalyst. (1) 1.0% CuO/CeO_2; (2) 5.0% CuO/CeO_2; (3) 10.0% CuO/CeO_2; (4) 15.0% CuO/CeO_2; (5) 10.0% CuO/CeO_2 (800 °C, 2 h); (6) 10.0% CuO/CeO_2 (900 °C, 2 h); (7) CeO_2.

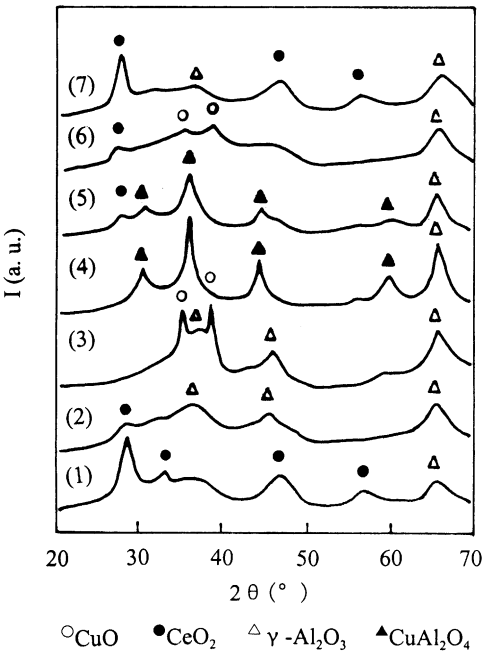

Fig. 5. XRD patterns of $CuO/\gamma\text{-}Al_2O_3$ catalyst. (1) 10.0% $CeO_2/\gamma\text{-}Al_2O_3$; (2) 5.0% $CuO/\gamma\text{-}Al_2O_3$; (3) 10.0% $CuO/\gamma\text{-}Al_2O_3$; (4) 10.0% $CuO/\gamma\text{-}Al_2O_3$ (800 °C, 2 h); (5) 10.0% CuO-10.0% $CeO_2/\gamma\text{-}Al_2O_3$ (800 °C, 2 h); (6) 10.0% CuO-2.0% $CeO_2/\gamma\text{-}Al_2O_3$; (7) 10.0% CuO-10.0% $CeO_2/\gamma\text{-}Al_2O_3$.

lower temperatures. In contrast, the reduction profiles of CuO/CeO_2 catalysts calcined at 800 °C were similar to those of the catalysts calcined at normal activation temperatures (500 °C, 2 h), but the reduction peak only occurred at higher temperatures. When CuO/CeO_2 catalysts were calcined at 900 °C for 2 h, the low-temperature peak changed to a large shoulder and loose peak, likely due to the worsening disperse state of CuO and a larger CuO crystalline.

There was a diffraction peak of $CeO_2/\gamma\text{-}Al_2O_3$ between 2θ 28.5, 47.5° and 2θ 45.6, 66.5° at the CuO loading of ≤5.0 wt.% (Fig. 5). One diffraction peak of CuO occurred between 2θ 35.5 and 38.7° additional to the $CeO_2/\gamma\text{-}Al_2O_3$ diffraction peak at the CuO loading of more than 5.0 wt.%. After calcination at 800 °C for 4 h, the crystalline diffraction peak of $CuO/\gamma\text{-}Al_2O_3$ became even smaller, and a spinel structure of $CuAl_2O_4$ was observed between 2θ 31.3, 36.9 and 37.9° for 10.0% $CuO/\gamma\text{-}Al_2O_3$. This may indicate that a solid phase reaction occurred between CuO and $\gamma\text{-}Al_2O_3$ at 800 °C, which caused the formation of $CuAl_2O_4$ from some of CuO and $\gamma\text{-}Al_2O_3$.

After addition of 2.0 or 10.0 wt.% CeO_2 to $CuO/\gamma\text{-}Al_2O_3$ catalyst, the diffraction peak of CuO became smaller or disappeared and the catalytic activity was improved, suggesting a close relationship between the catalytic activity and CuO particles. In order to prove the deduction, 10.0 wt.% CeO_2 was added to $CuO/\gamma\text{-}Al_2O_3$ catalysts and then calcined at 800 °C for 4 h. As shown in line 5 of Fig. 5, the $CuAl_2O_4$ diffraction peaks became much smaller, indicating that the CeO_2 addition restrained $CuAl_2O_4$ formation. Lines 6 and 7 of Fig. 5 also show that the CuO diffraction peak was present after addition of 2.0 wt.% CeO_2 to $CuO/\gamma\text{-}Al_2O_3$, but disappeared after addition of 10.0 wt.% CeO_2. It was likely that the CeO_2 reduced the average crystalline grain of CuO and increased the catalytic activity.

As shown in the TPR profiles of $CuO/\gamma\text{-}Al_2O_3$ catalyst, there was one reduction peak for each CuO loadings of 1.0, 5.0, 10.0 wt.% and pure CuO at peak temperatures of 264.6, 276, 317 and 392 °C, respectively (lines 1–4, Fig. 6). However, the reduction temperature range of $CuO/\gamma\text{-}Al_2O_3$ catalysts became wider and hydrogen consumption peak shifted towards

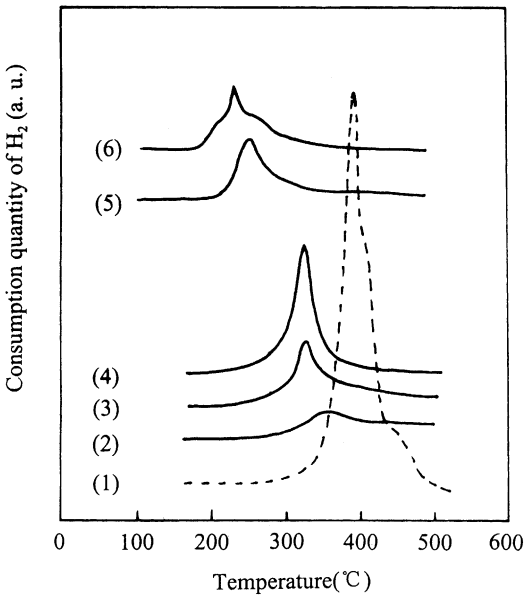

Fig. 6. TPR patterns of CuO/γ-Al_2O_3 catalyst. (1) CuO($Cu(NO_3)_2$ (500 °C, 2 h); (2) 1.0% CuO/γ-Al_2O_3; (3) 5.0% CuO/γ-Al_2O_3; (4) 10.0% CuO/γ-Al_2O_3; (5) 10.0% CuO-2.0% CeO_2/γ-Al_2O_3; (6) 10.0% CuO-10.0% CeO_2/γ-Al_2O_3.

the direction of lower temperatures, indicating that due to the interaction between CuO and γ-Al_2O_3, a change of CuO dispersion state had occurred. In contrast, although addition of 2.0 wt.% CeO_2 resulted in only one reduction peak, there were three reduction peaks with the addition of 10.0 wt.% CeO_2 at 215, 230 and 270 °C (line 6). Presumably, the peak at 215 °C was caused by the reduction of highly dispersed CuO, and the peaks at 230 and 270 °C were due to the reduction of different crystalline CuO particles interacting with CeO_2.

3.4. XPS surface analysis

The CuO/CeO_2 catalyst with a loading of 1.0 wt.% CuO had only Ce $3d_{5/2}$ (eV) but not Cu $2p_{3/2}$ (eV) binding energy (Table 3). By comparison, with a loading of 5.0 wt.% CuO the CuO/CeO_2 catalyst had the Cu $2p_{3/2}$ binding energy of 932.79 and 934.11 eV, indicating that CuO existed on the CeO_2 surface mainly as Cu^{2+} (934.4 eV) and Cu^{+} (932.6 eV). This could be related to the strong interaction between the redox couple (Ce^{4+}/Ce^{3+}) and CuO [17,18]. When CuO loading was more than 5.0 wt.% and the CuO/CeO_2 catalysts were calcined at 800 and 900 °C for 2 h, CuO existed on the CeO_2 surface mainly as Cu^2. Therefore, the state of CuO existence on the CeO_2 surface was dependent on the CuO loading and calcination temperature.

Table 3
Binding energy of XPS experimental results

Catalyst	Cu $2p_{3/2}$ (eV)	O 1s (eV)	Ce $3d_{5/2}$ (eV)
1.0% CuO/γ-Al_2O_3	935.0	533.7	
10.0% CuO/γ-Al_2O_3	935.0	533.6	
10.0% Cu/γ-Al_2O_3	932.7	533.4	
10.0% CuO-2.0% CeO_2/γ-Al_2O_3	935.0	533.4	882.5
10.0% CuO-10.0% CeO_2/γ-Al_2O_3	934.1	532.6	882.8
1.0% CuO/CeO_2		529.2	882.3
5.0% CuO/CeO_2	932.7, 934.1	529.7	882.9
15.0% CuO/CeO_2	930.2, 933.3	529.3	882.4
15.0% Cu/CeO_2	932.4	530.4	882.8
10.0% CuO/CeO_2 (800 °C, 2 h)	934.7	530.4	883.5
10.0% CuO/CeO_2 (900 °C, 2 h)	933.4	529.7	882.7

With a loading of 5.0–10.0 wt.% CuO, the CuO/γ-Al_2O_3 catalysts had the Cu $2p_{3/2}$ binding energy of 935.0 eV (Table 3), which was similar to Cu^{2+} (934.4 eV) and the same as $CuAl_2O_4$ (935.0 eV) but higher than CuO (934.1 eV) (Table 4), indicating some CuO existed as $CuAl_2O_4$ after heating at 800 °C for 1 h. Addition of 2.0 wt.% CeO_2 did not change the Cu $2p_{3/2}$ binding energy of CuO/γ-Al_2O_3 catalyst (935.0 eV). After the CeO_2 addition increased to 10.0 wt.%, the Cu $2p_{3/2}$ binding energy of the catalyst was slightly reduced to 934.1 eV and the CuO existed on the γ-Al_2O_3 surface mainly as Cu^{2+}.

After reduction, the Cu $2p_{3/2}$ binding energy of CuO/γ-Al_2O_3 and CuO/CeO_2 catalysts was equal to

Table 4
Binding energy of some compounds

Compound	Cu $2p_{3/2}$ (eV)	O 1s (eV)	Ce $3d_{5/2}$ (eV)	Reference
$CuAl_2O_4$	935.0	531.1		[13]
CuO	934.4	530.3		[14]
Cu_2O	932.6	530.8, 531.9		[13]
Cu	932.8			[14]
CeO_2			881.7	[15]

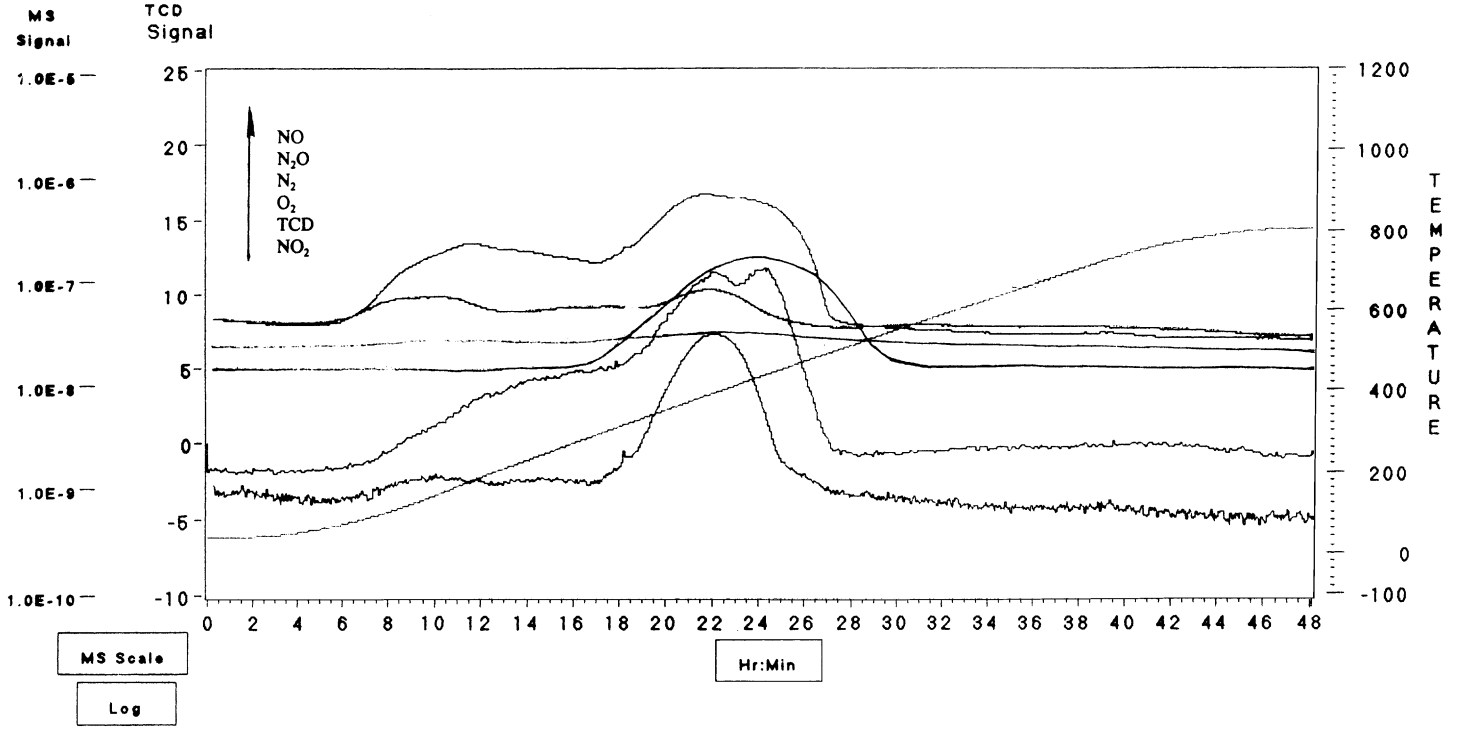

Fig. 7. NO-TPD spectra of CeO_2. NO ($m/e = 30$), N_2O ($m/e = 44$), N_2 ($m/e = 28$), O_2 ($m/e = 32$), NO_2 ($m/e = 46$).

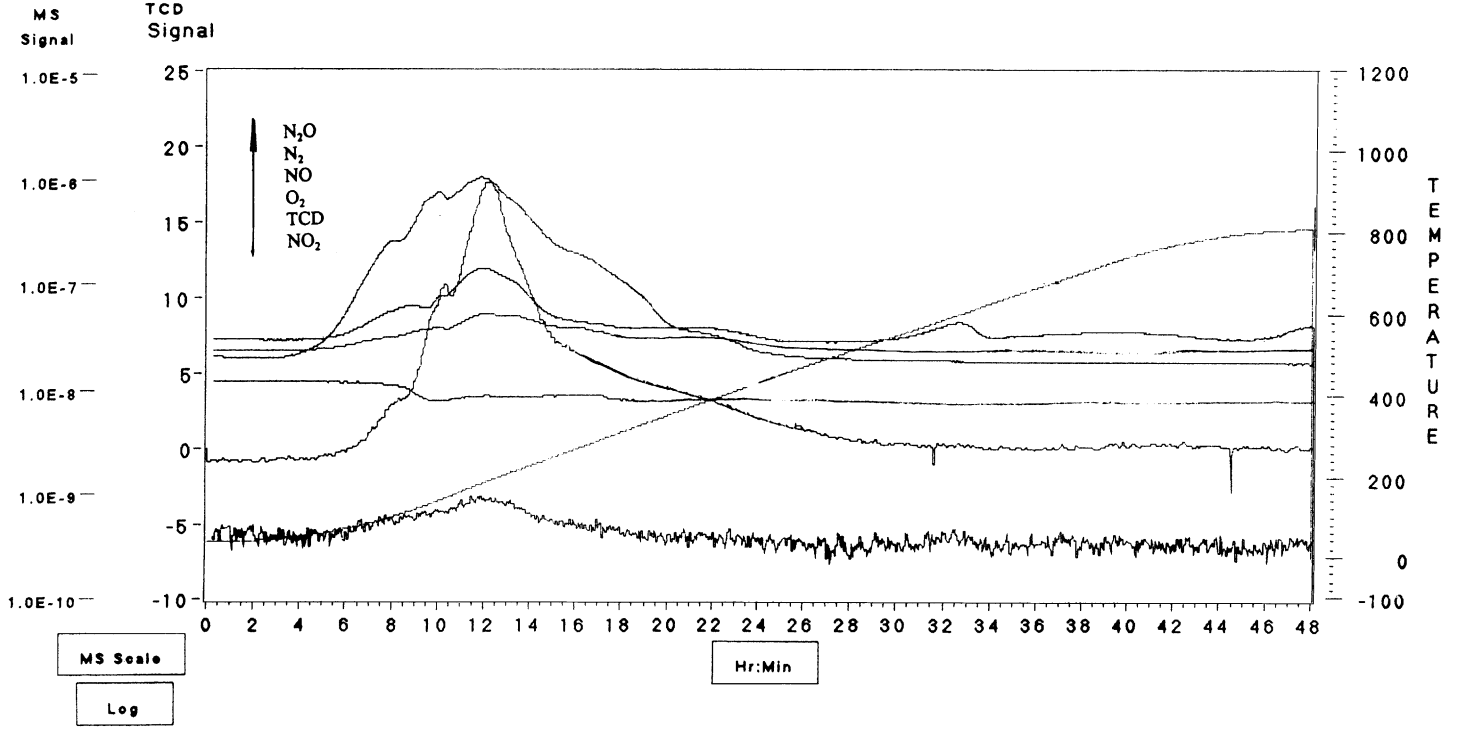

Fig. 8. NO-TPD spectra of CuO/CeO_2. NO ($m/e = 30$), N_2O ($m/e = 44$), N_2 ($m/e = 28$), NO_2 ($m/e = 46$).

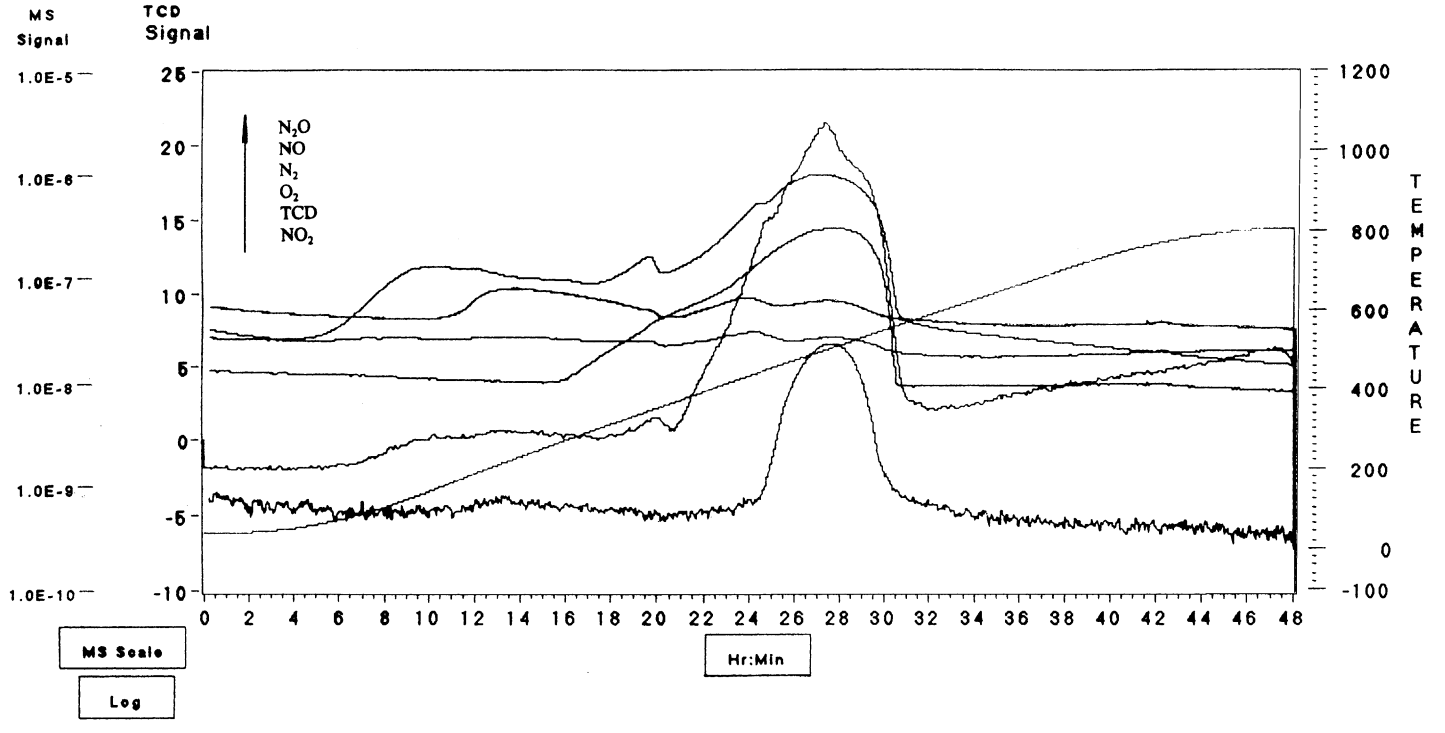

Fig. 9. NO-TPD spectra of γ-Al_2O_3. NO ($m/e = 30$), N_2O ($m/e = 44$), N_2 ($m/e = 28$), O_2 ($m/e = 32$), NO_2 ($m/e = 46$).

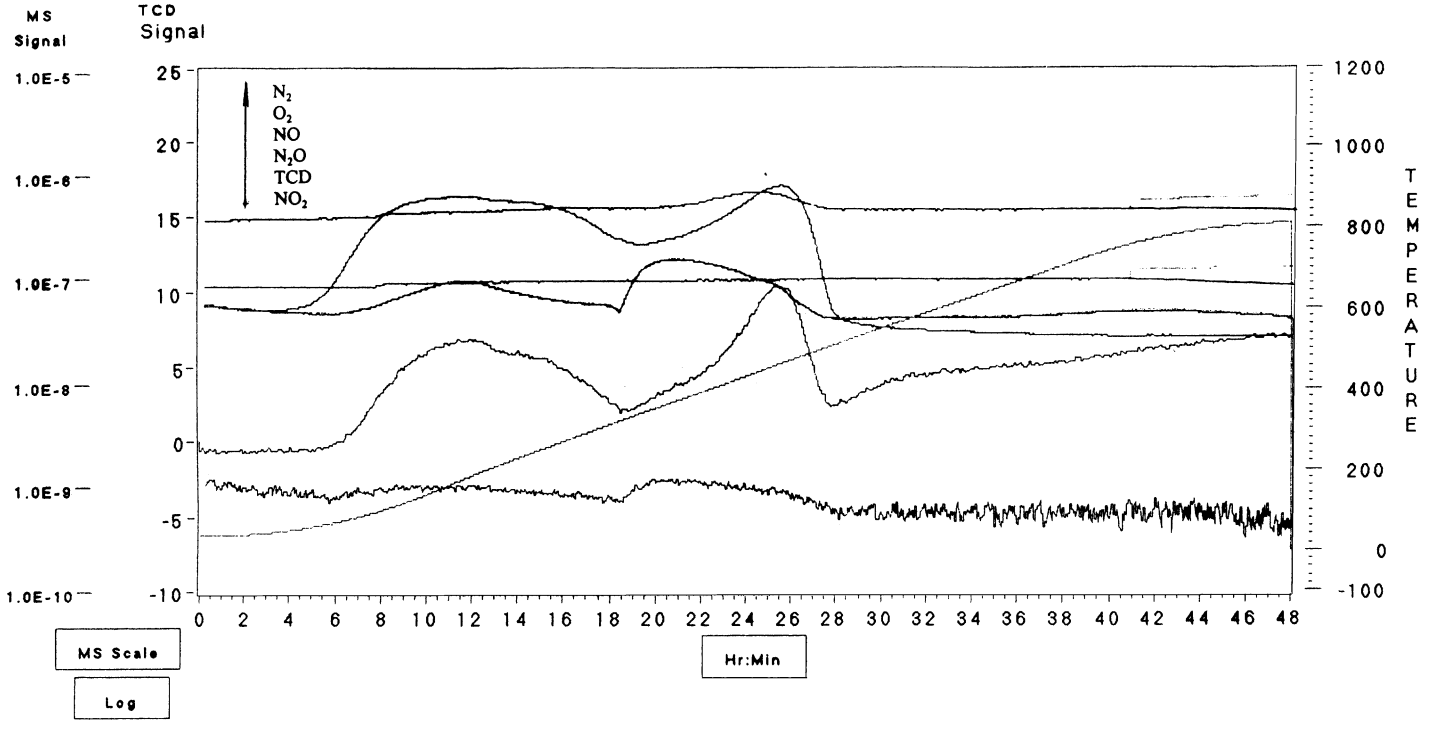

Fig. 10. NO-TPD spectra of CuO/γ-Al_2O_3. NO ($m/e = 30$), N_2O ($m/e = 44$), N_2 ($m/e = 28$), NO_2 ($m/e = 46$).

932.7 and 932.4 eV, respectively. By comparison, the standard Cu binding energy was the same as the binding energy of metal Cu.

3.5. TPD of the support and catalyst surfaces with adsorbed NO

After the CeO_2 and CuO/CeO_2 surfaces adsorbed NO, the thermal desorption process took place as a decomposition reaction, but desorption products were more complicated and usually determined using a mass spectrometer. The adsorption of NO by a CeO_2 support surface is shown in Fig. 7. The mass spectrometer tracking found five desorption species (N_2O, $m/e = 44$; N_2, $m/e = 28$; O_2, $m/e = 32$; NO_2, $m/e = 46$; NO, $m/e = 30$). The NO desorption process had three desorption peaks, i.e. three NO adsorbing states on the CeO_2 surface—two strongly and one weakly at 160, 360 and 460 °C, respectively. The NO adsorption by CuO/CeO_2 catalyst surfaces is shown in Fig. 8. During the NO desorption process, there were four desorption peaks at 70, 135, 150 and 260 °C, respectively, of which two were small peaks (one main peak and one shoulder peak), indicating that the NO adsorbed by CuO/CeO_2 catalysts surfaces was easy for decomposition and desorption. It was obvious that the desorption peak temperature of NO by CuO/CeO_2 catalyst was lower than that of CeO_2, which means that NO decomposition activity by CuO/CeO_2 was higher than by CeO_2. Fig. 8 also shows that the N_2O desorption peak was in lower temperature ranges. Namely, the NO + CO reaction produced N_2O at low temperatures. In addition, from two examined samples, N_2 was never detected, likely due to a very high background concentration of N_2 and very low concentrations of NO and N_2O. In other words, N_2 formed by further dissociation was negligible. Nevertheless, the thermal desorption products of CuO/CeO_2 did not produce O_2 desorption peak while its TPD process detected NO, N_2O and N_2. It was likely that NO decomposition produced atomic oxygen (O) that dispersed or entered into the bulk of Cu [19,20]. The desorption of atomic oxygen could only occur at high temperatures.

Figs. 9 and 10 show the TPD spectra of γ-Al_2O_3 support and CuO/γ-Al_2O_3 catalyst surfaces that adsorbed NO. After the γ-Al_2O_3 surface adsorbed NO, the process of NO desorption produced three desorption peaks, i.e. three adsorbing states of NO on the γ-Al_2O_3 surface, where two weak states were at 110, 340 °C and one strong state at 500 °C. After the CuO/γ-Al_2O_3 catalyst surface adsorbed NO, however, the NO desorption produced only two desorption peaks at 130 and 460 °C. The lower desorption peak temperatures of NO by CuO/γ-Al_2O_3 than by γ-Al_2O_3 indicate that the NO decomposition activity of the former was higher than that of the latter. Similar to CuO/CeO_2 catalyst, the thermal desorption products of CuO/γ-Al_2O_3 catalyst did not produce O_2 desorption peak while the TPD process detected NO, N_2O and N_2. In contrast, the thermal desorption products of γ-Al_2O_3 could determine O_2 desorption peak but not N_2 desorption peak, while its TPD process detected NO, N_2O and O_2. These results suggest that the conversion of N_2O into N_2 needs much higher temperatures. After CuO/γ-Al_2O_3 catalyst surfaces adsorbed NO, the mass spectrometer was able to detect the desorption product N_2, i.e. the NO + CO reaction by CuO/γ-Al_2O_3 catalyst. As shown in the TPD data, N_2O and N_2 were produced at low and high temperatures, respectively.

4. Conclusion

CuO/CeO_2, CuO/γ-Al_2O_3 and CuO-CeO_2/γ-Al_2O_3 catalysts had higher activities for the NO+CO reaction than those without CuO addition. The activities were related to the amount of CuO loading and combination of the supports, and are shown as the following order: 5.0% CuO/CeO_2 < 10.0% CuO/CeO_2 < 10.0% CuO-10.0% CeO_2/γ-Al_2O_3 < 10.0% CuO-2.0% CeO_2/γ-Al_2O_3 < 10.0% CuO-10.0% CeO_2/γ-Al_2O_3 (800 °C, 2 h)<1.0% CuO/CeO_2 < 10.0% CuO/γ-Al_2O_3 < 10.0% CuO/γ-Al_2O_3 (800 °C, 2 h).

Different CuO loading and support combinations caused changes in surface area, reduction peaks, Cu $2p_{3/2}$ (eV) binding energy and NO decomposition activity of the catalysts. An increase in CuO loading decreased the surface area of CuO/CeO_2 and CuO/γ-Al_2O_3. Two reduction peaks for CuO/CeO_2 and one reduction peak for CuO/γ-Al_2O_3 were observed, compared to three reduction peaks for the CeO_2-modified CuO/γ-Al_2O_3 catalyst. At 5.0 wt.% CuO loading the Cu $2p_{3/2}$ (eV) binding energy of CuO/CeO_2 catalyst displays the properties of Cu^{2+}

and Cu^{+}, whereas at 5.0–10.0 wt.% CuO loading the Cu $2p_{3/2}$ (eV) binding energy of CuO/γ-Al_2O_3 displays the properties of Cu^{2+}. After addition of 10.0 wt.% CeO_2, the Cu $2p_{3/2}$ (eV) binding energy was similar to or slightly lower than that before the addition. Species NO, N_2O, N_2, O_2 and NO_2 were detected during the thermal desorption of NO adsorbed on CeO_2 and γ-Al_2O_3 supports, whereas species NO, N_2O, N_2 and NO_2 were detected during thermal desorption of NO adsorbed on CuO/CeO_2 and CuO/γ-Al_2O_3 catalysts. Peak temperatures of NO desorption by the catalysts were lower than that by the supports, i.e. NO decomposition activity of the catalysts was higher than that of the supports.

References

[1] K. Taylor, Catal. Rev. Sci. Eng. 35 (1993) 457.
[2] M. Shelf, Catal. Rev. Sci. Eng. 11 (1975) 1.
[3] H. Bosch, F. Janssen, Catal. Today 2 (1988) 369.
[4] K. Sakurai, Y. Okamoto, T. Imanaka, S. Teranishi, Bull. Chem. Soc. Jpn. 49 (1976) 1732.
[5] W.C. Hekker, A.T. Bell, J. Catal. 84 (1983) 200.
[6] S.H. Oh, C.C. Zickel, J. Catal. 128 (1991) 526.
[7] J.M. Schwartz, L.D. Schmidt, J. Catal. 18 (1994) 22.
[8] J.R. Gonzalez-Velasco, J. Entrena, J.A. Gonzalez-Marcos, J.I. Gutierrez-Ortiz, M.A. Gutierrez-Ortiz, Appl. Catal. B: Environ. 3 (1994) 191.
[9] H. Muraki, K. Yokota, Y. Fujitani, Appl. Catal. 48 (1989) 93.
[10] M. Iwamoto, H. Yahiro, Y. Torikal, T. Yoshioka, N. Mizuno, Chem. Lett. (1990) 1967.
[11] G. Centi, S. Perathoner, Appl. Catal. A 132 (1995) 179.
[12] D. Panayotov, L. Dimitrov, M. Khristova, L. Petrov, D. Mehandjiev, Appl. Catal. B: Environ. 6 (1995) 61.
[13] B.R. Strohmeier, D.E. Leyden, R.S. Field, D.M. Hercules, J. Catal. 94 (1985) 514.
[14] V. Di Castro, C. Furlani, M. Gargano, Appl. Surf. Sci. 28 (1987) 270.
[15] B. Harrison, A.F. Diwell, C. Hallett, Platinum Met. Rev. 32 (1988) 73.
[16] H. Kobayashi, N. Takezawa, M. Shimokawabe, Stud. Surf. Sci. Catal. 16 (1983) 697.
[17] J.G. Nunan, H.J. Robota, M.J. Cohn, S.A. Bradley, J. Catal. 133 (1992) 309.
[18] R. Monte, P. Fornasiero, J. Kaspar, P. Rumori, G. Gubitosa, M. Graziani, Appl. Catal. B: Environ. 24 (2000) 157.
[19] K.Y. Simon Ng, D.N. Belton, S.J. Schmieg, G.B. Fisher, J. Catal. 146 (1994) 394.
[20] J. Kaspar, C. Leitenburg, P. Fornasiero, A. Trovarelli, M. Graziani, J. Catal. 146 (1994) 136.